

# Investigation of pressure effects on elastic parameters of isotropic and anisotropic MgO

A. DOGHMANE\*, S. DOUAFER, Z. HADJOUR

*Laboratoire des Semi-Conducteurs, Département de Physique, Faculté des Sciences, Université Badji-Mokhtar, BP 12, Annaba, DZ-23000, Algérie.*

In this paper, we investigate the effects of increasing pressure,  $P$  from 0 to 150 GPa on elastic properties as reflection coefficients, acoustic signatures, acoustic wave velocities,  $V$ , and elastic moduli,  $M$  in isotropic and anisotropic MgO. It is found that, at a given pressure, all the investigated acoustic parameters depend on crystallographic orientations. Moreover, the analysis and quantification of pressure effects lead to the determination of semi-empirical formulas applicable to all acoustic parameters with different characterising constants. These relations for propagating Rayleigh, longitudinal and transverse waves velocities  $V_i$  and for Young's (shear) modulus  $M$  are of the form:  $V_i = V_{i0} + A_i \exp(P/t_i)$  and  $M_p = M_{p0} + B_p \exp(-P/t_p)$ , respectively; where  $A_i$ ,  $t_i$ ,  $B_p$ ,  $t_p$  are characteristic constants for velocities and elastic moduli; the subscript  $(o)$  represents the corresponding parameters at zero pressure; the subscripts  $(i = R, L, T)$  represent the propagating Rayleigh, longitudinal and transverse waves. These formulas are important for the prediction of elastic parameters at any given pressure and vice versa.

(Received September 19, 2013; accepted November 13, 2014)

*Keywords:* MgO, pressure, velocities, elastic constants, anisotropy

## 1. Introduction

MgO, one of the oldest ceramics, is receiving renewable interest due to the development of new growth techniques and the increasing potential of this material in numerous modern applications in various fields as semiconductors, nuclear power, steel industry, etc.... This ceramic material may exist in isotropic or anisotropic structural forms as a result of preparation conditions and techniques. The structural simplicity and broad spectrum of stability at high pressure-temperature of MgO have attracted a spectacular evolution in the number of applications and the high performances of such a ceramic material. Therefore, a fine comprehension, a continuous understanding of its structure and the means of obtaining it, in a reliable, robust and profitable way, are required.

Mechanically, MgO is described by its density as well as its elastic moduli [1, 2] that can be characterized via static or dynamic methods. The latter, mainly ultrasonic, are nondestructive; they require the knowledge of density,  $\rho$ , and velocities. However, these values become dispersive if the material is kept under pressure. In this context, we investigate not only elastic properties of

isotropic MgO but also the influence of pressure and anisotropy on these properties (reflection coefficients, acoustic signatures, Rayleigh velocities, elastic constants).

## 2. Calculation Procedure and Conditions

The details of calculation procedure, which could be found elsewhere [3-5], consists of several steps: (i) calculation of the reflection coefficient  $R(\theta)$ , (ii) calculation of the acoustic signature,  $V(z)$ , (iii) treatment of  $V(z)$  by fast Fourier transform, FFT, (iv) determination of the velocity of propagating modes and (v) repetition of all previous steps (i-iv) for each value of the pressure and every crystallographic orientation.

The simulation conditions are those usually used experimentally in the case of a reflexion scanning acoustic microscope: a half opening angle of lens of  $50^\circ$ , an operating frequency  $f = 140$  MHz and water as a coupling liquid whose wave velocity,  $V_{\text{liq}} = 1500$  m/s and density,  $\rho = 1000$  kg/m<sup>3</sup>. The MgO acoustic parameters used in this investigation are listed in Table 1 [6].

Table 1. Acoustic parameters (longitudinal velocity,  $V_L$ , transverse velocity,  $V_T$ ) of isotropic and anisotropic MgO [6]

P (GPa)	$\rho$ (g /m <sup>3</sup> )	MgO <sub>iso</sub>		MgO <sub>&lt;100&gt;</sub>		MgO <sub>&lt;110&gt;</sub>		MgO <sub>&lt;111&gt;</sub>	
		$V_L$ (m/s)	$V_T$ (m/s)	$V_L$ (m/s)	$V_T$ (m/s)	$V_L$ (m/s)	$V_T$ (m/s)	$V_L$ (m/s)	$V_T$ (m/s)
0	3486	9580	5910	9140	6310	9730	5360	9920	5690
5	3590	9920	6040	9650	6290	10010	5700	10120	5900
10	3685	10250	6200	10140	6300	10280	6010	10330	6140
20	3856	10810	6450	10970	6320	10770	6320	10710	6540
40	4144	11740	6810	12370	6330	11630	6330	11370	7200
60	4386	12440	7060	13470	6300	12300	6300	11880	7740
80	4596	13050	7250	14390	6290	12910	6290	12370	8150
100	4785	13590	7400	15240	6230	13440	6230	12790	8560
125	4998	14130	7550	16140	6160	14000	6160	13200	9000
150	5189	14160	7690	16890	6110	14450	6110	13540	9400

### 3. Investigation of pressure effects on isotropic MgO

#### 3.1 Pressure effects on $R(\theta)$

To show the influence of pressures on reflection coefficients,  $R(\theta)$ , we first calculated these functions at various pressures (0 – 150 GPa) for isotropic MgO; the obtained curves are displayed in Fig. 1. For a better clarity of curve representation and since  $R(\theta)$  is a complex function, we separated the amplitude curves (Fig. 1a) from those of the phase (Fig. 1b). Then, for different pressures, we superposed the real parts and the imaginary parts as a function of the incidence angles,  $\theta_i$ .

From fig. 1a, representing the amplitude of  $R(\theta)$  as a function of incidence angle,  $\theta_i$ , one can clearly observe: (i) a first fluctuation in amplitude when the angle of incidence reaches the values of critical longitudinal angles,  $\theta_L$ , (ii) a shift in  $\theta_L$  towards lower values when the pressure increases, (iii) a second increase in amplitude when the angle of incidence reaches the values of the critical transverse angles,  $\theta_T$ , (iv) between  $\theta_L$  and  $\theta_T$  the amplitude of  $R(\theta)$  remains constant and (iv) beyond  $\theta_T$  the amplitude of  $R(\theta)$  increases to reach unity corresponding to total reflection.

From fig. 1b, representing the phase of  $R(\theta)$  as a function of  $\theta_i$ ; it can easily be noticed that a  $2\pi$  transition (for  $P = 0$  GPa) is obtained. This transition occurs at the critical angle,  $\theta_R$ , that corresponds to the Rayleigh mode, which is the most important one under the present simulating conditions. Thus, Rayleigh mode dominates all other modes leading to the fact that the longitudinal critical angle,  $\theta_L$ , is not very noticeable.

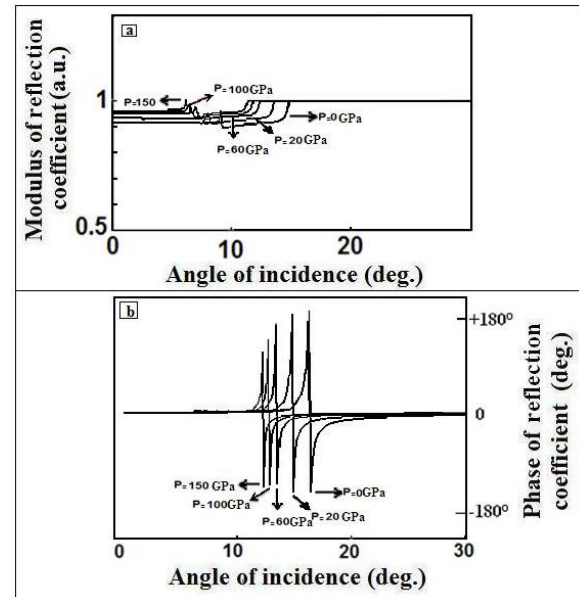


Fig. 1. Amplitude (a) and phase (b) of reflection coefficients as a function of incidence angles at different pressure values for isotropic MgO.

It can also be seen that the amplitude of the transition in Rayleigh mode phase becomes less than the usual  $2\pi$  value as the pressure increases. Whereas, the position, i.e., the value of  $\theta_R$  moves towards lower values with increasing  $P$  (a similar behaviour to that noticed with  $\theta_L$  in Fig. 1a). Moreover, it is clear that all modes are generated with angles lower than  $20^\circ$ . These critical angles strongly depend on the simulation conditions, in particular coupling liquid densities [7].

#### 3.2 Pressure effects on $V(z)$

Acoustic signatures can be obtained experimentally, via a scanning acoustic microscope, by recording the variation of amplitude,  $V$ , of the signal as a function of

displacement,  $z$ , from the lens towards the sample. These signatures, which depend on  $R(\theta)$ , can also be calculated from the spectral angular model [8]. The curves, thus calculated, at various pressure values are represented in Fig. 2a for the isotropic material,  $\text{MgO}_{\text{iso}}$ . It is clear that all the curves of  $V(z)$  present an oscillatory behaviour, with a spatial period  $\Delta z$ , due to constructive and destructive interferences between propagating modes. It is noted that, as the pressure changes,  $V(z)$  curves differ in amplitudes as well as in periods,  $\Delta z$ . In amplitudes, the curves attenuate more rapidly for higher pressures, see e.g.,  $P = 150$  GPa. In periods, we observe an initial shift of successive maxima which leads to larger periods for higher pressures.

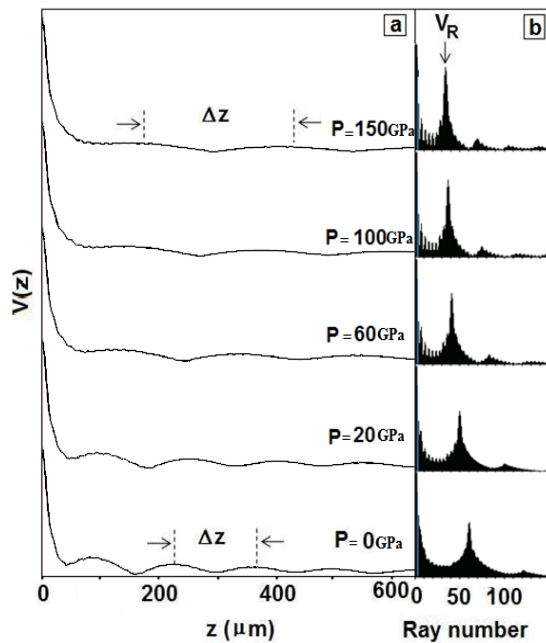


Fig. 2. Acoustic signatures (a) and fft spectra (b) for isotropic MgO, at different pressure values.

The FFT spectral analysis of these periodic  $V(z)$  curves is shown in Fig. 2b. These spectra are characterized by a principal peak representing the most dominating mode which is that of Rayleigh, under the present conditions. However, the efficiency of this mode, represented by its height [7], is more important for the highest pressure of 150 GPa. Moreover, a small shift for the principal ray is observed putting into evidence the differences in spatial periods  $\Delta z$  obtained in  $V(z)$  curves.

#### 4. Study of anisotropy effects

In order to investigate anisotropy effects on elastic properties of MgO we considered different orientations (Table 1):  $\text{MgO}_{\langle 100 \rangle}$ ,  $\text{MgO}_{\langle 110 \rangle}$  and  $\text{MgO}_{\langle 111 \rangle}$ . It should be

noted that we determined, for all these cases, reflections coefficients as well as acoustic materials signatures at different pressure values. Since the behaviours of obtained results are identical and reproducible, we only report some representative curves.

Typical obtained results of  $R(\theta)$  for isotropic and anisotropic MgO are illustrated in Fig. 3 for uncharged ( $P = 0$  GPa; Fig. 3a) and maximally charged ( $P = 150$  GPa; Fig. 3b) in terms of modulus (---), referred to the left hand side axis and phase (—) referred to the right hand side axis, as a function of incidence angles.

It is clear that all critical angles,  $\theta_L$ ,  $\theta_T$ , and  $\theta_R$  corresponding to longitudinal, transverse and Rayleigh modes, respectively, differ from one orientation to the other. They also show significant changes between charged and uncharged materials as well between isotropic and anisotropic MgO.

The calculated acoustic signatures,  $V(z)$ , for isotropic MgO and  $\text{MgO}_{\langle 100 \rangle}$ ,  $\text{MgO}_{\langle 110 \rangle}$  and  $\text{MgO}_{\langle 111 \rangle}$  are shown in Fig. 4a ( $P = 0$  GPa) and Fig. 4b ( $P = 150$  GPa). The effects of pressure and anisotropy can clearly be seen as discrepancies between amplitudes and  $\Delta z$  periods in  $V(z)$  curves.

### 5. Quantification of pressure effects on acoustic parameters

#### 5.1. Rayleigh velocity dispersion with pressure

It is well established that the spatial period  $\Delta z$  is related to Rayleigh velocity by the expression via the following relation [5]:

$$V_R = \frac{V_{liq}}{\sqrt{1 - \left(1 - \frac{V_{liq}}{2f\Delta z}\right)^2}} \quad (1)$$

Hence, any shift in the position of principal ray,  $\Delta z$ , in FFT spectra leads a variation in the corresponding Rayleigh velocity,  $V_R$ . Therefore, the above mentioned observations with pressure and anisotropy effects can be quantified through the determination of Rayleigh velocities,  $V_R$ , in every case. This is justified by the fact that such velocities depend on periods  $\Delta z$  which are a consequence of the periodic behavior of  $V(z)$  curves; the latter being dependent on  $R(\theta)$ .

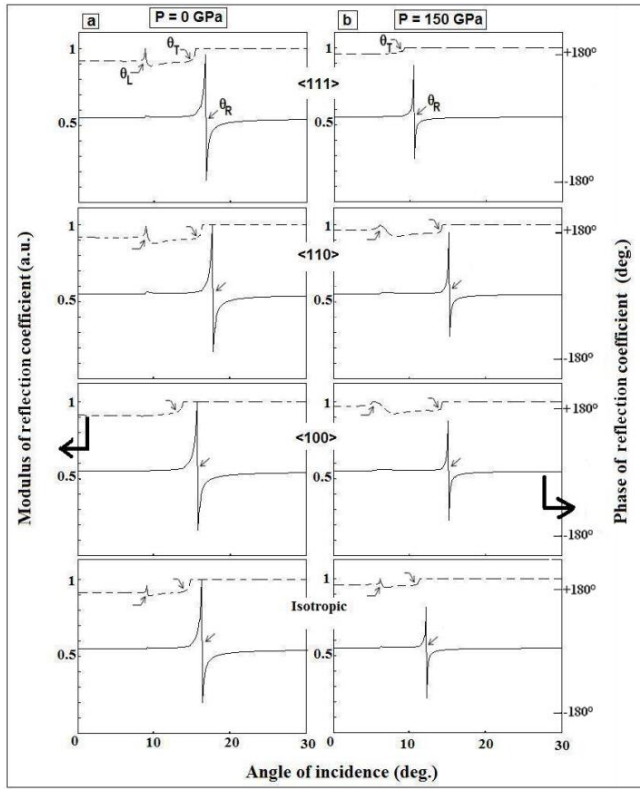


Figure 3. Reflection coefficients as a function of incidence angles for isotropic and anisotropic MgO; (a)  $P = 0$  GPa and (b)  $P = 150$  GPa.

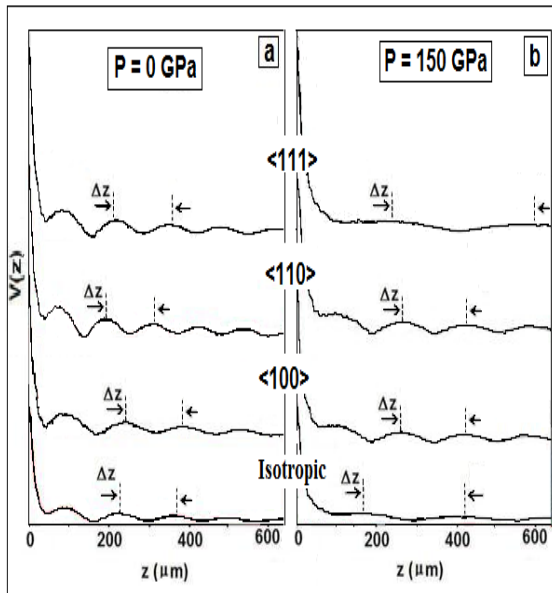


Fig. 4.  $V(z)$  curves for isotropic and anisotropic MgO; (a)  $P = 0$  GPa and (b)  $P = 150$  GPa.

The deduced  $V_R$  values are better illustrated in Fig. 5 as a function of pressure. It can be noticed that there is a sharp initial increase of  $V_R$  up to  $P = 80$  GPa followed by slower dependence. This variation is due to the crystalline structure of MgO which becomes more compact by compressing it. As the pressure increases, the atoms get closer which leads to a better wave propagation initially;

whereas, for higher pressures the atoms cannot get too close leading to a kind of velocity saturation.

In order to analytically quantify such behaviours, we deduced a relation between Rayleigh velocity and pressure, via curve fitting, of the form:

$$V_R = 7356 - 1960e^{\left(\frac{-P}{105}\right)} \quad (2)$$

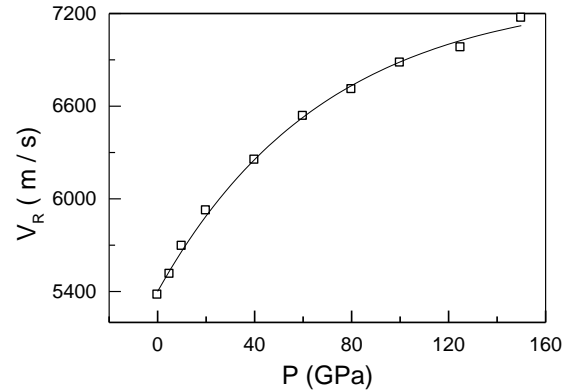


Fig. 5. Dispersion of Rayleigh velocity with pressure; the continuous line (—) represents the best fit.

It should be noted that similar behaviours were deduced for longitudinal and transverse velocities; the following relations were also deduced:

$$V_L = 16108 - 6476e^{\left(\frac{-P}{105}\right)} \quad (3)$$

$$V_T = 7868 - 1947e^{\left(\frac{-P}{68}\right)} \quad (4)$$

A close look at the above relations shows clearly that they all follow the same variations that take the following analytical form:

$$V_i = V_{i0} + A_i e^{\left(\frac{-P}{t_i}\right)} \quad (5)$$

with the subscript ( $i = R, L, T$ ) representing the propagating Rayleigh, longitudinal and transverse mode, respectively, and  $A_i$  as well as  $t_i$  being characteristic constants.

## 5.2. Elastic constant variations with pressure

Elastic constants can be expressed in terms of according to propagating wave velocities  $V_T$ ,  $V_L$  and/or  $V_R$  [9-11]. Thus, we calculated the Young's modulus,  $E$ , and shear modulus,  $G$ , for MgO under various pressures, by using the following familiar formulas:

$$E_1 = \rho V_T^2 \left( \frac{3\rho V_L^2 - 4\rho V_T^2}{\rho V_L^2 - \rho V_T^2} \right) \quad (6)$$

$$G_1 = \rho V_T^2 \quad (7)$$

$$E_2 = 3\rho V_R^2 \quad (8)$$

$$G_2 = 1.54\rho V_R^2 \quad (9)$$

Typical obtained results are plotted in Fig. 6 for Young's modulus as a function of pressure; similar behavior was also obtained for shear modulus.

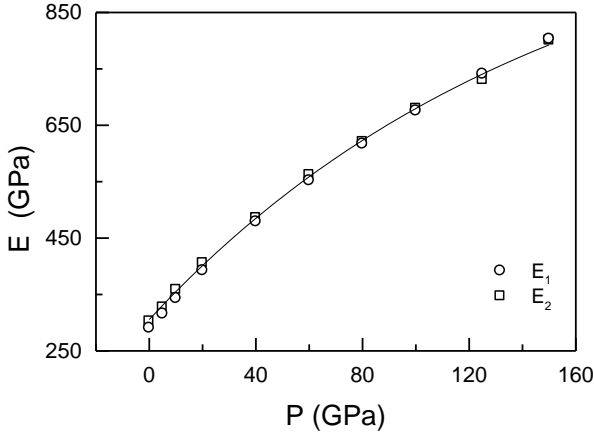


Fig. 6. Pressure effects on Young's modulus  $e_1$  ( $\circ$ , eqn. 6) and  $e_2$  ( $\square$ , eqn. 8); the continuous line (—) represents the best fit.

It is clear that as the pressure increases we notice an initial sharp increase followed by a slower variation. In fact, when the pressure applied to MgO increases from 0 to 150 GPa,  $E$  increases from 302 to 800 GPa and the shear modulus from 116 to 308 GPa. The curve fitting led to an exponential variation similar to that of velocities; it was found that:

$$E = 1082 - 777e^{\left(\frac{-P}{152}\right)} \quad (10)$$

$$G = 409 - 286e^{\left(\frac{-P}{148}\right)} \quad (11)$$

The above relations of elastic moduli,  $M$ , (Young's or shear modulus) follow similar variations that take the following form:

$$M_p = M_{p0} + B_p e^{\left(\frac{-P}{t_p}\right)} \quad (12)$$

where the subscript  $(0)$  represents the corresponding parameter at a null pressure, and  $B_p$ ,  $t_p$  are characteristic constants for elastic moduli. These relations are of great importance in the prediction of specific applications; it

would be possible to predict the stress that the device should undergo by just knowing its elastic parameters and vice versa.

## 6. Conclusions

In this work, acoustic parameters of isotropic and anisotropic MgO were studied under various pressure values (0-150 GPa). Elastic parameters (reflection coefficients, acoustic signatures, Rayleigh velocities, Young's modulus and shear modulus) were calculated for all cases. It has been shown that these parameters change with increasing pressure. The variations of velocities and elastic constants were expressed by exponential semi-empirical relations. The importance of these formulas lies in the prediction of elastic parameters for any given pressure and vice versa.

## References

- [1] B.H. Flowers, E. Mendoza, Properties of Matter, John Wiley, New York, 1970.
- [2] S. Amelo, A. V. Goldade, U. Rabe, V. Scherer, B. Bhushan, W. Arnold, Thin Solid Films, **393**, 75 (2001).
- [3] I. Al-Surayhi, A. Doghmane, Z. Hadjoub, Adv. Mater. Res. **811**, 77 (2013)
- [4] Z. Hadjoub, I. Beldi, A. Doghmane, Comptes Rendus de Physique, **8**, 948 (2007).
- [5] J. Kushibiki, N. Chubachi, IEEE Trans. Sonics and Ultrasonics, **SU-32**, 189 (1985).
- [6] R. B. Karki, J. L. Stixrude, S.J. Clark, M.C. Warren, G. J. Ackland, J. Crainj, Am. Mineralogist, **82**, 51 (1997).
- [7] A. Doghmane, Z. Hadjoub, K. Alami, J. M. Saurel, J. Attal, J. Acoust. Soc. Am., **92**, 1545 (1992).
- [8] C. J. R. Sheppard, T. Wilson, App. Phys. Lett., **38**, 858 (1981)
- [9] M. Doghmane, F. Hadjoub, Z. Hadjoub, A. Doghmane, Mater. Lett., **61**, 813 (2007).
- [10] G. A. D. Briggs, W. Arnold, Advances in Acoustic Microscopy, Kluwer Academic, New York, 1996.
- [11] I. A. Viktorov, Rayleigh and Lamb Waves, Plenum Press, New York, 1967.

\*Corresponding author: a\_doghmane@yahoo.fr